Caving 2026 – A van As, D Cumming-Potvin & J Wesseloo (eds)

doi:10.36487/ACG_repo/2645_33

Fragmentation assessment in caving mining: operational evidence from Chuquicamata underground mine

Carlo Divasto Vergara [a,*], Giuseppe Barindelli Pizarro [a], Rodrigo Quiroz Alegría [a]

[a] *Chuquicamata, Codelco, Chile*

Abstract

A quantitative fragmentation assessment is presented for the Chuquicamata underground mine based on the integration of operational evidence obtained from drawpoint granulometric mapping, records of secondary breakage of oversized fragments, and production extraction reports. The study focuses on the macroblocks MB N01-S01, MB N02-N03, and MB S02-S03, using a comprehensive multi-source database collected between 2019 and 2025. This database comprises more than 7,500 drawpoint inspections, 5,000 geometric measurements of rock fragments, and a continuous record of secondary breakage events. This robust dataset enables a comprehensive evaluation of fragmentation behaviour at the drawpoint scale under deep caving mining conditions.

The analysis examines the relationship between observed fragmentation, the basic geotechnical units (BGUs) model and the extraction height, with the primary objective of identifying systematic trends in granulometric evolution as caving progresses. Furthermore, operationally derived fragmentation results are compared with the prognosis developed by SRK in 2021 for the first lift of extraction (Lift 1). The findings indicate that the measured fragmentation is consistently finer than projected across the analysed sectors, revealing critical deviations in specific units such as the Potassic East Porphyry unit, where models based on discrete fracture network and block caving fragmentation (DFN-BCF) methodology significantly overestimated the rock mass competency and blockiness. Moreover, the results suggest that the model algorithm underestimates the fines fraction due to the comminution process inherent to secondary fragmentation.

Fundamental contributions of this research include identifying a tendency towards more elongated geometries as fragment size increases, which contradicts the traditional spherical assumption commonly used in theoretical estimations. Additionally, the study demonstrates that recorded secondary breakage events constitute a more robust and statistically representative operational proxy for tracking the oversize fraction than visual drawpoint mapping, which is biased toward the fines fraction. Nevertheless, both the frequency of secondary breakage and P_{80} values from field mapping reflect a consistent tendency to progressively decrease as extraction height increases.

Keywords: *fragmentation, cave mining, drawpoint fragmentation, secondary breakage, operational data*

1 Introduction

Fragmentation assessment constitutes a fundamental pillar of caving mining as it is essential for understanding gravity flow behaviour and ensuring operational continuity at drawpoints. In this context, the particle size distribution of the extracted material not only dictates loading efficiency but also directly impacts materials handling strategies and the overall productivity of the mine.

The Chuquicamata underground mine (MCHS) is a world-class operation that uses the block caving method with macroblock variants. Production commenced in 2019 with the commissioning of the central macroblock, MB N01-S01. Since then, operations have scaled significantly through the successive incorporation of

[*] Corresponding author. Email address: cdiva001@codelco.cl

macroblocks MB N02-N03, MB S02-S03 and MB N41, consolidating an operational database of high value for geomechanical and fragmentation analysis.

Despite designs based on predictive models for primary and secondary fragmentation, experience in these active sectors has revealed discrepancies between initial projections and the actual conditions observed at the drawpoints. This technical gap becomes more pronounced as the extraction height increases, where fines generation and the evolution of the granulometric curve present challenges that traditional models – such as the Guajardo & Russo (2021) prognosis – fail to capture with sufficient accuracy. Specifically, these models often struggle to account for the complex comminution processes and the morphological characteristics of the rock mass under high-stress conditions.

This study aims to bridge this gap through a quantitative fragmentation analysis at MCHS, integrating over 7,500 granulometric inspections and a continuous record of secondary breakage events collected between 2019 and 2025. The work focuses on characterising the response of different basic geotechnical units (BGUs), evaluating the influence of extraction height, and validating the consistency of operational data against theoretical size distribution models to improve future production planning and infrastructure sizing.

2 Background information

This section outlines the operational and geological framework of MCHS to provide context for the subsequent fragmentation analysis. Figure 1 shows a plan view of the three primary macroblocks under evaluation: MB N01-S01, MB N02-N03 and MB S02-S03. This layout is superimposed on the BGU model to illustrate the spatial distribution of each geotechnical unit across the extraction level.

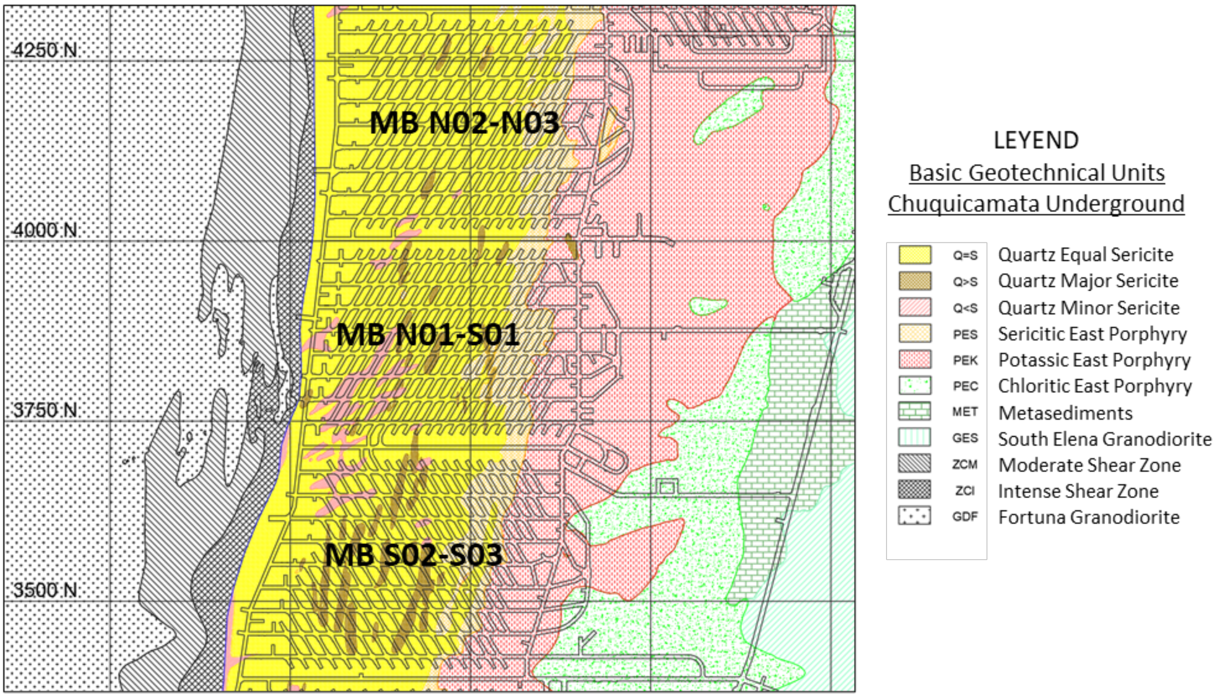

Figure 1 Plan view of the 2024 basic geotechnical unit model across the three primary macroblocks at Chuquicamata underground mine (Vega et al. 2024)

Furthermore, Table 1 summarises the mechanical properties of the intact for the three main BGUs within these sectors (Barindelli 2016, Barindelli 2018). The data include mean values for density, unconfined compressive strength (σ_c), indirect tensile strength (σ_t) and Young's modulus (E), establishing a geomechanical baseline for the study. Incorporating these parameters ensures that the fragmentation assessments accounts for the specific mechanical response of the rock mass, facilitating the identification of systematic trends in particle size evolution as cave extraction progresses.

Table 1 Intact rock properties by basic geotechnical unit (BGU) for the three primary macroblocks

Macroblock	BGU	Areal distribution (%)	Density (t/m^3)	σc (MPa)	σt (MPa)	E (GPa)
MB N01-S01	QIS	66	2.70	66	−2.0	20
	PES	30	2.69	72	−3.2	29
	PEK	4	2.61	95	−4.0	37
MB N02-N03	QIS	83	2.73	71	−5.4	44
	PES	16	2.66	74	−3.1	48
	PEK	1	2.62	95	−4.7	48
MB S02-S03	QIS	64	2.70	61	−3.5	30
	PES	18	2.67	70	−4.1	29
	PEK	18	2.62	88	−3.0	49

3 Methodological framework

To achieve the research objectives, a comprehensive methodological framework was implemented, integrating direct field mapping, mathematical modelling of fragmentation size distributions, and the systematic evaluation of historical operational datasets.

3.1 Geotechnical characterisation of macroblocks

The analysis was founded on the mechanical properties of the BGUs identified within macroblocks MB N01-S01, MB N02-N03 and MB S02-S03. The uniaxial compressive strength (UCS) parameter was integrated for the primary units: Quartz Equal Sericite (QIS), Sericitic East Porphyry (PES) and Potassic East Porphyry (PEK). This characterisation enables the correlation of intact rock competence with both fines generation rates and block sizes throughout the caving process.

3.2 Sampling and particle size distribution adjustment (Rosin-Rammler)

The fragmentation data collection protocol at the drawpoints used a dual validation system. This approach incorporated direct visual mapping for rapid field assessment, complemented by digital image analysis using Split-Desktop software to validate visual estimations and minimise observer bias. Regarding fines estimation, a 50% fines factor was assumed based on the default value of the software, without additional calibration. Further studies are currently under way on the conveyor belt system to improve the understanding and quantification of fines generation.

Furthermore, each granulometric dataset was mathematically fitted using the Rosin-Rammler distribution function (Vesilind 1980). This standardisation of individual inspections facilitated a rigorous comparison of the resulting particle size distribution curves against various prognoses across different extraction stages. The distribution is defined by the following expression:

$$P(x) = 100e^{-(x/x_0)^n} \quad (1)$$

where:

$P(x)$ = is the cumulative percentage retained on a sieve of size x

x_0 = is the characteristic size (size at which 36.8% of the material is retained)

n = is the uniformity index.

3.3 Morphometric analysis and shape factor

A specific morphometric study was conducted on rock fragments, categorising them into four size classes to evaluate their influence on gravity flow behaviour:

- Fine (with major axis <1 m)
- Medium (1–2 m)
- Coarse (2–3 m)
- Oversized (>3 m).

The three orthogonal axes (L: long, I: intermediate and S: short) were measured for each fragment. To define the shape and sphericity, the Sneed and Folk (1958) maximum projection sphericity (Ψ_p) was calculated:

$$\Psi_p = \sqrt[3]{\frac{S^2}{LI}} \quad (2)$$

where:

Ψ_p = is the maximum projection sphericity

S, I, L = short, intermediate, and long orthogonal axis, respectively.

Complementarily, the shape factor parameter introduced by Gy (1967) was employed to characterise the fragment geometry and its relationship with volume (V), defined by the expression:

$$f = \frac{V}{L^3} \quad (3)$$

where:

f = is the shape factor

V = is the volume

L = is the long axis.

These equations allow for a precise transition from linear measurements to volumetric estimations. By combining the calculated shape factor with the rock density, the mass of oversized fragments was accurately determined.

3.4 Secondary breakage analysis

As oversized fragments often cannot be directly measured during the standard granulometric mapping, secondary breakage records were used as indirect indicators of coarse fragmentation. Data were retrieved from the mine operations department which systematically logs all events associated with oversized fragment reduction. These events are categorised into three critical operational classes: hang-ups, brow boulders and floor boulders.

Based on technical literature regarding drawpoint design (e.g. Hadjigeorgiou and Lessard 2007), the geometric dimensions of the drawpoints and morphometric fragment analysis, an equivalent size range of 3.5–4.0 m was assigned as the minimum threshold for fragments prone to causing brow obstructions or hang-ups. Additionally, event frequency was quantified by calculating the tonnage between events.

3.5 Integration with production and extraction parameters

Finally, the compiled dataset – encompassing particle size distributions, secondary breakage events and fragment morphology – was cross-referenced with daily production records. This synchronisation allowed for the attribution of specific operational parameters, such as cumulative tonnage and extraction height, to each data point based on its recorded timestamp. This integration facilitates a temporal evolution analysis of fragmentation evolution.

4 Results

To ensure a coherent integration of the various data sources according to the previously described methodology, this section is structured into four fundamental pillars.

4.1 Fragment morphology and characterisation

The analysis of drawpoint fragment measurements aims to achieve two primary objectives: first, to characterise the shape factor and sphericity of the particles; and second, to assess the impact of these morphological features on the mass balance. A direct correlation between fragment size and a progressive loss of sphericity was identified.

4.1.1 Shape factor and sphericity

Morphological analysis was applied to four size classes defined in the methodology. Table 2 summarises the shape factor results by BGU and size class for the three macroblocks under study.

Table 2 Shape factor geometric relationships by basic geotechnical unit (BGU) and particle size class

Macroblock	BGU	Fine	Medium	Coarse	Oversized
MB N01-S01	QIS	0.35	0.25	0.20	0.18
	PES	0.37	0.26	0.24	0.13
	PEK	0.32	0.21	0.48	–
MB N02-N03	QIS	0.39	0.32	0.31	0.29
	PES	0.42	0.32	0.31	0.15
	PEK	0.38	0.30	–	–
MB S02-S03	QIS	0.39	0.36	0.36	–
	PES	0.42	0.31	0.27	0.17
	PEK	0.41	0.36	0.24	0.21

Figures 2 and 3 illustrate the sphericity distribution of the fragments plotted on a ternary diagram from Sneed and Folk (1958). A distinct transition toward elongated geometries is observed as the major axis length increases, suggesting that these morphological features significantly reduce material flowability.

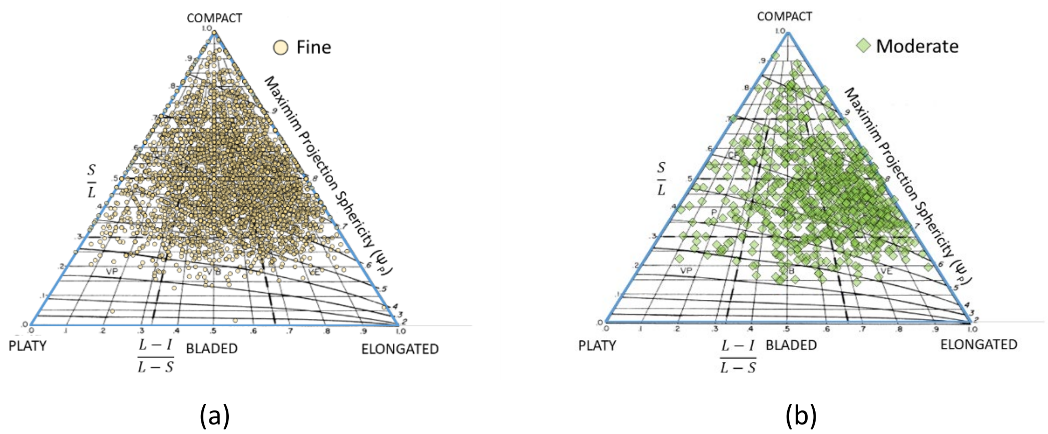

Figure 2 Distribution of fragment sphericity. (a) Fine size class; (b) Medium size class

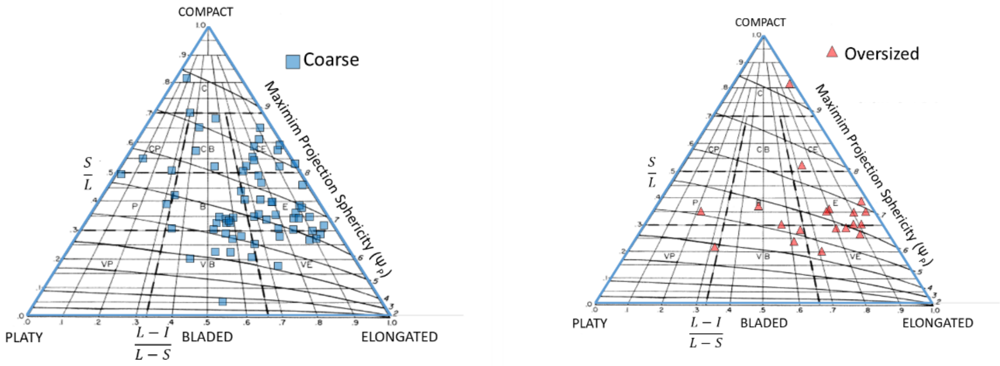

(a) (b)

Figure 3 Distribution of fragment sphericity. (a) Coarse size class; (b) Oversized size class

The comparative analysis between Figures 2 and 3 reveals a profound morphological shift as fragment size increases. While smaller particles (fine and medium classes) exhibit a well-distributed range of shapes in the ternary diagram, larger fragments – particularly in the oversize class – show a marked migration toward the elongated zone. This shape evolution suggests that larger blocks tend to preserve structural anisotropies of the rock mass, resulting in geometries that are significantly more prone to interrupting flow at the drawpoints. Consequently, the assumption of spherical geometry for secondary breakage volume estimations leads to a systematic overestimation of the actual fragment mass.

4.1.2 Impact on mass estimation

Applying the previously determined shape factors enabled a volumetric conversion of linear measurements, allowing for a precise estimation of individual fragment mass. This conversion is essential for the secondary breakage study, particularly regarding the predicted tonnage of oversized fragments.

To define the average size of fragments likely to trigger hang-ups and brow boulder events, gravity flow principles were evaluated. While studies such as those mentioned in Hadjigeorgiou and Lessard (2007) suggest ratios ranging from 3:1 to 6:1 between drawpoint width and the major axis of a fragment for free flow, operational evidence at MCHS indicates maximum fragment sizes at the drawpoint floor between 3.5 and 4.0 m. Given that the standard drawpoint opening at MCHS ranges from 4.8 to 5.2 m, a 3:2 ratio was derived for fragments capable of causing flow interruptions due to oversize events. This finding is consistent with operational observations and established literature.

Table 3 summarises the tonnage estimation as a function of the maximum axis and the shape factor, providing an average mass baseline for oversized fragments. Compared to an ideal sphere (where $f = 0.52$), these results show that oversized fragments at Chuquicamata have a mass 40–50% lower due to their elongated shapes.

Table 3 Volume and tonnage estimation for oversized fragments based on shape factor

Shape factor	Fragment volume (m^3)		Fragment tonnage (t)	
	Axis 3.5 m	Axis 4 m	Axis 3.5 m	Axis 4 m
0.15	6.4	9.6	17.4	25.9
0.2	8.6	12.8	23.2	34.6
0.3	12.9	19.2	34.7	51.8

4.2 Fragmentation behaviour by basic geotechnical unit

Results correlating directly to specific geotechnical units are derived exclusively from in situ granulometric mapping at the drawpoints. This represents the only operational stage where the predominant BGU within the muckpile can be directly identified and recorded.

However, as illustrated in Figure 1, the spatial distribution of the various BGUs is heterogeneous across the sectors. Consequently, the varying data density may introduce a sample bias in units with limited representation. Despite this, Tables 4 and 5 summarise the geometric mean of the P_{80} passing and the fines fraction (defined as material <10 cm), respectively. Both parameters are tabulated by BGU and categorised by extraction height levels: 10 m, 20 m, 40 m, 80 m and 200 m.

Table 4 Geometric mean of the P_{80} passing size in metres by basic geotechnical unit and extraction height

Macroblock	UGB	10 m	20 m	40 m	80 m	200 m
MB N01-S01	QIS	1.25	1.10	0.76	0.68	0.34
	PES	1.11	0.89	0.76	0.77	0.29
	PEK	1.20	–	–	–	–
MB N02-N03	QIS	0.76	0.93	0.77	0.44	0.24
	PES	0.75	0.73	0.71	0.52	0.18
	PEK	–	–	–	–	–
MB S02-S03	QIS	0.77	0.69	0.60	0.32	–
	PES	0.70	0.76	0.63	0.38	–
	PEK	0.62	0.77	0.73	0.38	–

Table 5 Geometric mean of the cumulative percentage of fines content (<10 cm) by basic geotechnical unit and extraction height

Macroblock	UGB	10 m	20 m	40 m	80 m	200 m
MB N01-S01	QIS	3.30	2.70	13.20	15.46	46.68
	PES	1.78	3.29	16.38	14.41	56.95
	PEK	0.08	–	–	–	–
MB N02-N03	QIS	16.29	14.54	19.89	29.95	56.57
	PES	11.30	18.46	18.64	27.76	54.46
	PEK	–	–	–	–	–
MB S02-S03	QIS	17.7	22.02	27.80	48.40	–
	PES	13.07	17.02	22.14	36.55	–
	PEK	17.17	16.69	20.62	28.16	–

A comparative analysis of the data presented in Tables 4 and 5 reveals a distinct behaviour between the coarse and fines fraction of the fragmentation. While the P_{80} values show relative homogeneity across the different BGUs at equivalent extraction heights, the fines content exhibits significant lithological and extraction dependency.

This trend suggests that the generation of fines is more sensitive to the specific geomechanical properties of each BGU, such as intact rock strength. Consequently, the percentage of fines serves as a more effective discriminator for assessing the geomechanical response of the units during the caving process despite maintaining a similar P_{80} profile.

Additionally, a consistent temporal trend is observed, as the extraction height increases from 10 to 200 m, there is a progressive reduction in the P_{80} values coupled with a systematic increase in fines content. This evolution is indicative of the secondary fragmentation and comminution processes occurring within the draw column. As the rock mass travels a greater distance through the gravitational flow, the fragments are subjected to higher inter-particle stresses and grinding, leading to a finer overall particle size distribution.

Furthermore, the variability in fines content, particularly during early cave draw, can also be attributed to the preferential movement of finer material through the cave column. As demonstrated by Castro et al. (2022), fine material can flow significantly faster than the coarse fraction due to inter-particle percolation. This rapid migration implies that fines percolate downwards through the coarser rock mass, meaning that the fines extracted early on do not necessarily originate from the same theoretical extraction height as the accompanying coarse rock. Consequently, a higher variability in the effective extraction height for finer materials for a given tonnage is expected, acting concurrently with the secondary fragmentation processes described above.

4.3 Secondary breakage behaviour by extraction height

This section examines the dynamics of secondary breakage across the macroblocks, focusing on the individual performance of drawpoints as extraction progresses. A correlation by BGU was excluded from this analysis, as direct geological mapping of hang-up and brow boulder events is operationally precluded by rigorous safety protocols. Furthermore, floor boulders were excluded from the drawpoint-specific analysis due to potential inaccuracies in their spatial attribution; in operational practice, these fragments are frequently relocated from their original source to clear the loading area. This logistical handling often results in inconsistent records within the tracking system, compromising the reliability of assigning these events to a specific drawpoint.

To establish a baseline, the secondary breakage event frequencies updated as of March 2026 are presented in Table 6. Note that floor boulders are included here for total frequency context but were excluded from subsequent spatial and temporal trend analyses. The dataset details the total event counts and the effectiveness of each intervention, where effectiveness is defined as the successful restoration of the drawpoint's operational availability.

Table 6 Secondary breakage event frequency and operational effectiveness by macroblock

Macroblock	Event category	Total events (N)	Effectiveness (%)
MB N01-S01	Hang-up	4,299	85
	Brow boulder	2,376	93
	Floor boulder	2,246	100
MB N02-N03	Hang-up	5,185	92
	Brow boulder	4,580	92
	Floor boulder	976	100
MB S02-S03	Hang-up	7,427	89
	Brow boulder	6,123	90
	Floor boulder	1,288	100

The cumulative tonnage extracted between consecutive hang-up and brow boulder events was analysed across 10 m extraction height intervals. To ensure statistical representativeness, this assessment exclusively considered instances where active material flow was recorded between successive events; consequently, drawpoints with no recorded secondary breakage events were excluded from the analysis. Figures 4–6 illustrate the observed trends for each macroblock using box-and-whisker plots. In these plots, the central box represents the interquartile range (spanning the first and third quartiles, Q1 and Q3), with the median indicated by a central line, while the whiskers extend to the minimum and maximum observed values.

A positive slope in these figures indicates an improvement in drawpoint flowability, as a higher tonnage can be extracted before a new secondary breakage intervention is required.

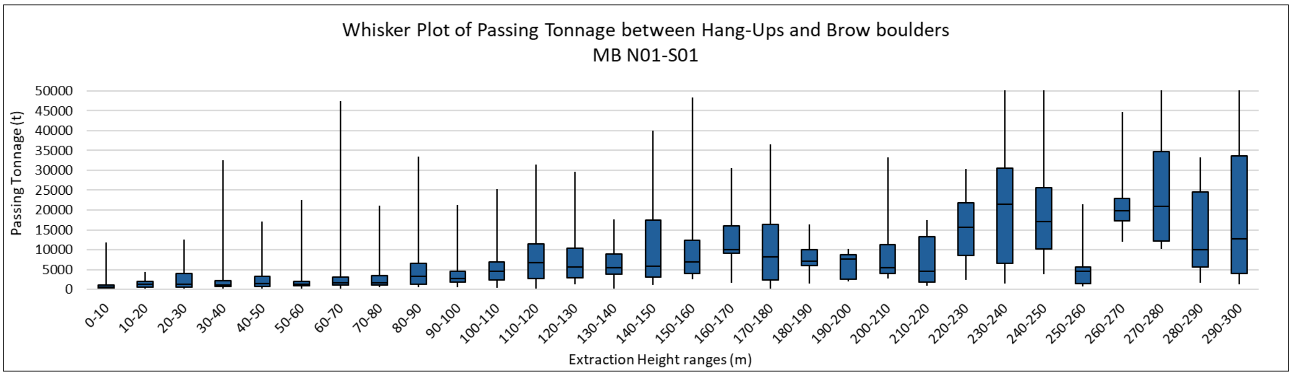

Figure 4 Inter-event tonnage distribution for hang-ups and brow boulders by extraction height range – MB N01-S01

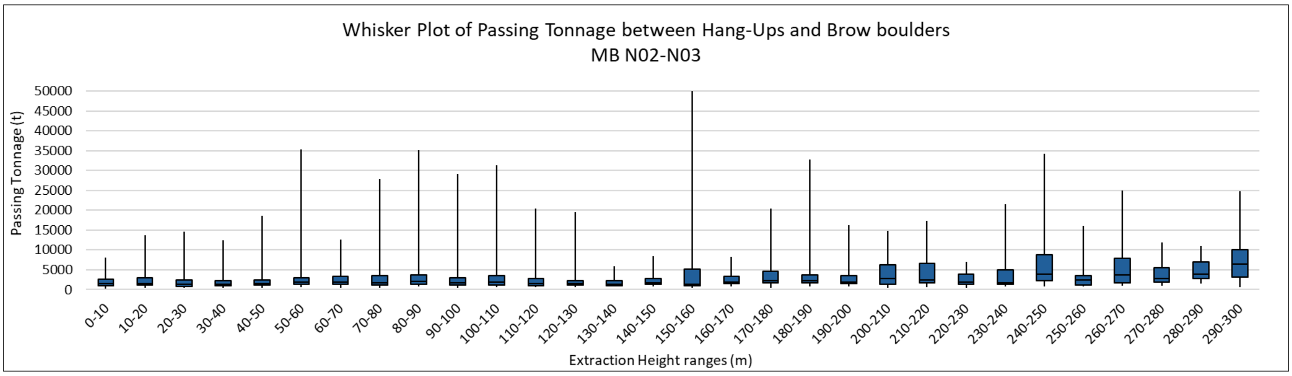

Figure 5 Inter-event tonnage distribution for hang-ups and brow boulders by extraction height range – MB N02-N03

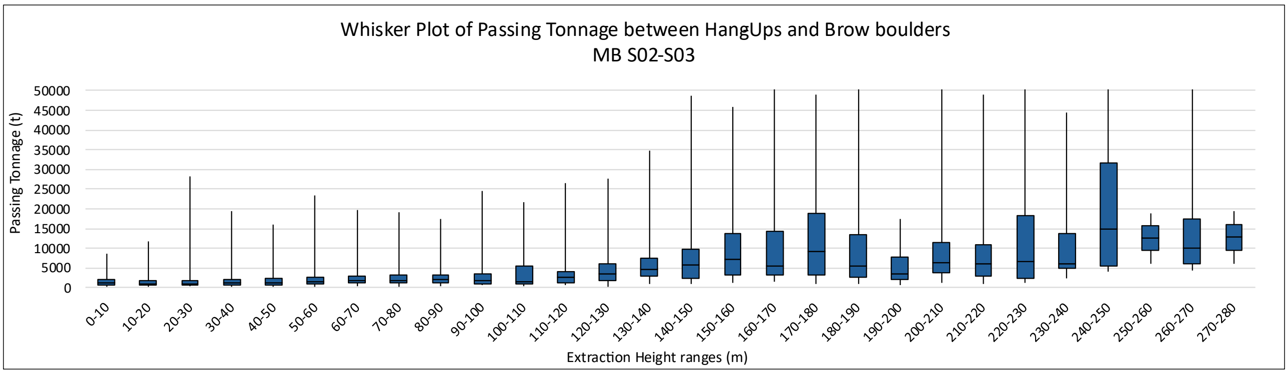

Figure 6 Inter-event tonnage distribution for hang-ups and brow boulders by extraction height range – MB S02-S03

To quantify the oversize fraction within the total mass flow, a conversion was performed by assuming a representative mass of 30 tonnes for each recorded hang-up and brow boulder event. This 30-tonne representative mass is not an arbitrary value; it represents a mean value obtain from the volumetric integration derived from the previous morphological analysis (Table 3). By comparing this estimated event tonnage against the actual tonnage extracted within each 10 m height interval, the relative mass contribution of oversized fragments was determined.

The results of this correlation are presented in Figures 7–9, which illustrate the evolution of the oversize percentage as a function of extraction height for each macroblock using box-and-whisker plots. In these plots, the central box represents the interquartile range (spanning the first and third quartiles, Q1 and Q3), with the median indicated by a central line, while the whiskers extend to the minimum and maximum observed values.

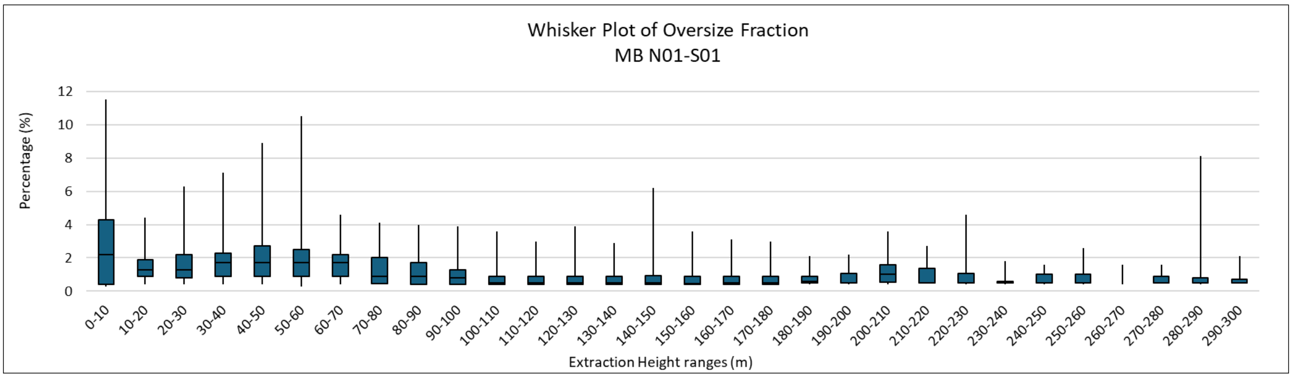

Figure 7 Whisker plot of oversize fraction through extraction height ranges considering drawpoints with events only – MB N01-S01

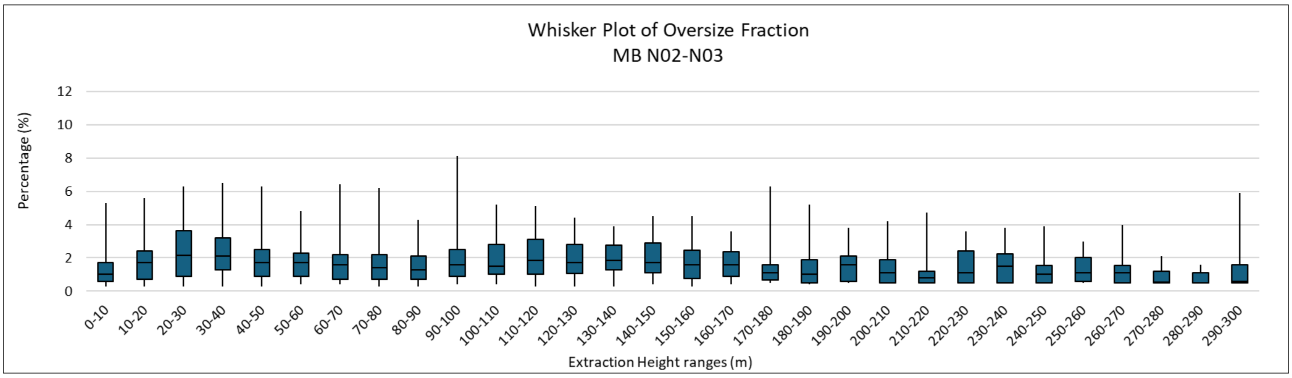

Figure 8 Whisker plot of oversize fraction through extraction height ranges considering drawpoints with events only – MB N02-N03

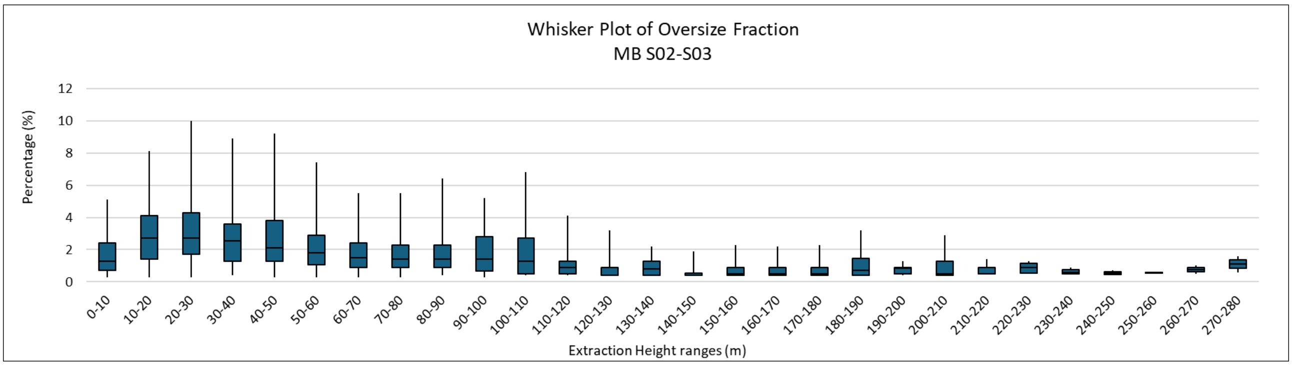

Figure 9 Whisker plot of oversize fraction through extraction height ranges considering drawpoints with events only – MB S02-S03

Across all monitored macroblocks, the data reveal that the oversize fraction is highest during the early stages of extraction, primarily driven by the arrival of primary fragmentation. However, as the draw column height advances, a steady stabilisation or decay in oversize fraction is observed. This trend suggests that while the frequency of events may be high initially, the actual mass contribution of oversized fragments decreases significantly as the sector matures.

4.4 Comparison with fragmentation prognosis

To evaluate the accuracy of theoretical estimates against operational reality, a benchmark analysis was conducted using the study developed by SRK Consulting (Guajardo & Russo, 2021), titled 'Final Report for Fragmentation Estimation for the First and Second Level Macroblocks of the Chuquicamata Underground Mine'. This study employed a hybrid methodology integrating discrete fracture network (DFN) and block caving fragmentation (BCF) to project primary and secondary fragmentation across 12 macroblocks in the first level and the central macroblocks of the second level.

To establish a direct and technically consistent comparison with the results obtained in this study, the analysis metrics were aligned. First, the volumetric P_{80} values from the prognosis were converted to linear units by applying a shape factor of 0.52, equivalent to a spherical geometry. Second, an equivalence was established between SRK's fines limit (0.001 m^3) and the 10 cm parameter used in our granulometric mapping. Third, as SRK reports the oversize fraction for blocks exceeding 2 m^3, this value was adjusted in the comparative tables to reflect the behaviour of blocks larger than 20 m^3. This 20 m^3 threshold is established as the operational volumetric equivalent for oversized fragments, approximating the volume of a minimum oversize block (~22.3 m^3 calculated using a spherical shape factor of 0.52 and a 3.5 m characteristic dimension). This limit aligns closely with the average volume of 17.2 m^3 derived from the comprehensive geometry database in Table 3, which corresponds directly to the representative 30-tonne mass calculated in Section 4.3. Furthermore, as there is no direct correlation between the recorded secondary breakage events and the BGUs, a variable range is presented as the comparative element. This range exclusively considers drawpoints where such secondary breakage events have been documented, ensuring that the operational baseline reflects the specific areas where fragmentation challenges were encountered.

Tables 7–9 contrast the average values of the P_{80}, fines percentage and oversize fraction observed versus projected, allowing for the identification of model deviations relative to current flow maturity.

Table 7 Comparative analysis of fragmentation parameters by basic geotechnical unit (BGU) for Macroblock N01-S01

BGU	Metric	Guajardo & Russo (2021)				Current study			
		20 m	40 m	80 m	200 m	20 m	40 m	80 m	200 m
QIS	P_{80} (m)	1.4	1.4	1.3	1.2	1.1	0.8	0.7	0.3
	Fines <10 cm (%)	14.4	14.9	16.1	18.4	2.7	16.2	15.5	46.7
	Oversize >20 m^3 (%)	1.3	1.3	1.1	0.9	1.2	1.5	1.0	0.9
PES	P_{80} (m)	1.2	1.2	1.1	1.0	0.9	0.8	0.8	0.3
	Fines <10 cm (%)	14.5	15.1	16.3	18.9	3.3	16.4	14.4	56.9
	Oversize >20 m^3 (%)	1.4	1.4	1.1	1.0	1.2	1.5	1.0	0.9
PEK	P_{80} (m)	2.5	2.5	2.4	2.2	–	–	–	–
	Fines <10 cm (%)	14.2	14.7	15.5	17.6	–	–	–	–
	Oversize >20 m^3 (%)	13.6	13.4	12.8	11.8	–	–	–	–

Table 8 Comparative analysis of fragmentation parameters by basic geotechnical unit (BGU) for Macroblock N02-N03

BGU	Metric	Guajardo & Russo (2021)				Current study			
		20 m	40 m	80 m	200 m	20 m	40 m	80 m	200 m
QIS	P_{80} (m)	1.6	1.5	1.5	1.4	0.9	0.8	0.4	0.2
	Fines <10 cm (%)	14.5	15.1	16.4	18.7	15.5	19.9	29.9	56.6
	Oversize >20 m^3 (%)	3.5	3.4	2.6	2.6	1.6	1.6	1.2	1.2
PES	P_{80} (m)	1.7	1.7	1.5	1.5	0.7	0.7	0.5	0.2
	Fines <10 cm (%)	14.4	15.1	16.2	18.5	18.5	18.6	27.8	54.5
	Oversize >20 m^3 (%)	4.1	3.9	3.7	3.4	1.6	1.6	1.2	1.2
PEK	P_{80} (m)	–	–	–	–	–	–	–	–
	Fines <10 cm (%)	–	–	–	–	–	–	–	–
	Oversize >20 m^3 (%)	–	–	–	–	–	–	–	–

Table 9 Comparative analysis of fragmentation parameters by basic geotechnical unit (BGU) for Macroblock S02-S03

BGU	Metric	Guajardo & Russo (2021)				Current study			
		20 m	40 m	80 m	200 m	20 m	40 m	80 m	200 m
QIS	P_{80} (m)	1.5	1.5	1.4	1.3	0.7	0.6	0.3	–
	Fines <10 cm (%)	14.5	15.1	16.3	18.8	22.0	27.8	48.4	–
	Oversize >20 m^3 (%)	1.4	1.2	1.2	1.0	2.4	2.1	1.4	0.7
PES	P_{80} (m)	1.1	1.0	1.0	0.9	0.8	0.6	0.4	–
	Fines <10 cm (%)	14.5	15.1	16.3	19.1	17.0	22.1	36.6	–
	Oversize >20 m^3 (%)	0.08	0.06	0.05	0.06	2.4	2.1	1.4	0.7
PEK	P_{80} (m)	3.6	3.4	3.4	3.1	0.8	0.7	0.4	–
	Fines <10 cm (%)	14.4	14.7	15.7	17.5	16.7	20.6	28.2	–
	Oversize >20 m^3 (%)	21.2	20.0	19.8	17.1	2.4	2.1	1.4	0.7

The comparative analysis of the macroblocks reveals critical insights regarding the fragmentation and height ranges.

For MB N01-S01, the results are evaluated according to three primary metrics: P_{80} passing size, fines fraction and oversize percentage. Regarding the passing size P_{80}, statistical representativeness was achieved only for the QIS and PES units. In general, the measured fragmentation is finer than projected, with the magnitude of this deviation increasing as extraction progresses. In terms of the fines fraction, a significant discrepancy is observed in the first 20 m of extraction, where measured fines are substantially lower than the prognosis, and beyond this point the trend shift drastically as measured fines exceed the projected values. This early-stage variability strongly correlates with the complex dynamics of fines migration and inter-particle percolation discussed previously, which static models like DFN-BCF often fail to capture. Finally, the oversize projections provided by SRK fall within the ranges documented in the secondary breakage records. Notably, both the prognosis and field measurements exhibit a downward trend in this percentage relative to extraction height. While the PEK unit could not be directly compared due to lack measurements, its P_{80} and oversize percentage significantly exceed the values recorded for the QIS and PES units.

For MB N02-N03, the comparison focused exclusively on the QIS and PES units, as the PEK unit exhibits minimal areal coverage within this sector. This limited spatial distribution accounts for its exclusion from both the original prognosis and the current granulometric mapping. Based on the results in Table 8, the measured fragmentation is consistently finer than projected, with a deviation that widens from the early stages of extraction. Regarding the fines fraction, a strong correlation is observed within the 20–40 m range; however, beyond this interval, the trend shifts drastically as measured fines significantly exceed the projected values. Finally, the oversize projections demonstrate a high degree of correlation, with projected values falling within the ranges recorded in the field. Consistent with the findings for MB N01-S01, the overall fragmentation exhibits a clear downward trend in size relative to increasing extraction height.

For MB S02-S03, the comparison was extended to all three primary BGUs. Regarding the passing size P_{80}, and consistent with the MB N02-N03 assessment, a significant deviation is observed across all extraction height ranges. This discrepancy is most acute for the PEK unit, where the SRK prognosis predicted a substantially coarser fragmentation than what was recorded in the field. In terms of the fines fraction, operational measurements consistently exceed projected values, with the gap widening as extraction progresses.

Regarding the oversize fraction, the projections for the QIS and PES units demonstrate a strong correlation with measured secondary breakage records, although the PES results tend toward the lower boundary of the observed range. In contrast, the PEK unit exhibits a major anomaly; the projected oversize fraction is 10 times higher than the average values documented during operations. While the macroblock follows the general trend of granulometric decay relative to extraction height, the initial characterisation of the PEK unit represents the most significant deviation in the fragmentation model, suggesting that the macro-structuring of this unit was heavily overestimated.

5 Discussion

The discrepancy between the SRK prognosis and operational data highlights the limitations of both the theoretical fragmentation models and current measurement procedures. Several critical findings emerge from this gap: first, the overestimation of the PEK unit's fragmentation – evidenced in both P_{80} and oversize fractions – suggests that potassic alteration responds more dynamically to induced stresses than predicted by DFN-BCF models. Second, the evolution of fines fraction with the extraction height indicates an underrepresentation of comminution (grinding) within the secondary fragmentation algorithm, as well as a structural inability of these static models to simulate the preferential migration and percolation of fines through the draw column. Third, the systematic use of a spherical shape factor in models leads to a significant miscalculation of mass-to-volume ratio of boulders. Finally, the inherent bias in drawpoint mapping tends to underestimate the overall behaviour of rock mass, while the inconsistency of using 'floor boulders' as a proxy proves less reliable for estimating global oversize compared to comprehensive secondary breakage records.

Collectively, these observations indicate that fragmentation in block caving is a dynamic process that evolves significantly with flow maturity and cannot be fully captured by static engineering forecasts. The transition from theoretical projections to operational reality requires a calibration of shape parameters, drawpoint fragmentation and a shift toward using secondary breakage events as the primary sensor for fragmentation to improve the reliability of production planning, load–haul–dump performance estimates, and sizing of secondary reduction infrastructure.

6 Conclusion

The operational fragmentation is consistently finer than the 2021 SRK prognosis across all analysed macroblocks. This deviation is more pronounced in the macroblocks MB N02-N03 and MB S02-S03, where the gap between projected and observed P_{80} and fines fraction increases as the draw column matures, indicating that current algorithms may underestimate secondary fragmentation and fines migration.

The systematic use of a spherical shape factor in fragmentation models leads to a simplification of fragment mass that hinders a proper understanding of oversize material. Field evidence at Chuquicamata suggests a tendency towards more elongated geometries as fragment size increases.

The PEK unit represents the most significant model outlier; while predicted to be extremely coarse, field data show it to be substantially finer. Meanwhile, the projections for the QIS and PES units aligned more closely with the measured data.

Historical records of secondary breakage events provide a more robust and statistically representative proxy for tracking the oversize fraction than drawpoint mapping, which is often biased by fines.

Future fragmentation assessments must incorporate site-specific shape factors, height-dependent grinding factors, and fines calibration from conveyor belt system studies. Calibrating these parameters is essential to optimise operational process and ensure the efficiency of rock-breaking systems in subsequent macroblocks and mine lifts.

Acknowledgement

The authors would like to thank Codelco Chuquicamata for the support provided during this study. Special gratitude is extended to the superintendencies within the Mining Resources and Development Management (GRMD) for providing the operational information required for this research.

Use of artificial intelligence disclosure statement

In the preparation of this work, the authors used Gemini 3 Flash (Google) to translate and refine language from Spanish to English and ensure stylistic consistency throughout the manuscript. The authors have reviewed the content and edited it where required and take full responsibility for said content.

References

Barindelli, G 2016, *Propiedades de Roca Intacta Macrobloques Centrales (Intact Rock Properties of Central Macroblocks)*, Informe SGT-INF-001/2016, Superintendencia Geotecnia, Gerencia Recursos Mineros & Desarrollo, Mina Subterránea, División Chuquicamata de Codelco-Chile.

Barindelli, G 2018, *Estimación de las Propiedades Geotécnicas Macrobloques N2 al N4 y S2 al S3 y Prognosis de Propiedades Geotécnicas Macrobloques N5 al N7 y S4 al S7, Lift 1 (Estimation of Geotechnical Properties for Macroblocks N2 to N4 and S2 to S3 and Prognosis of Geotechnical Properties for Macroblocks N5 to N7 and S4 to S7, Lift 1)*, Informe GRMD-SPMS-INF-005/2018, Superintendencia Planificación Mina Subterránea, División Chuquicamata de Codelco-Chile.

Castro, R, Arancibia, L & Gómez, R 2022, 'Quantifying fines migration in block caving through 3D experiments', *International Journal of Rock Mechanics and Mining Sciences*, vol. 151, no. 105033, pp. 1365–1609, https://doi.org/10.1016/j.ijrmms.2022.105033

Guajardo, C & Russo, A 2021, *Reporte Final de la Estimación de Fragmentación para los Macrobloques del Primer y Segundo Nivel de Minera Chuquicamata Subterránea (Final Report of the Fragmentation Estimation for the First and Second Level Macroblocks of the Chuquicamata Underground Mine)*, SRK Consulting, Santiago, N° Proyecto: 01-2400-01, 42p.

Gy, PM 1967, *Memoires du Bureau de Recherches Geologiques Minieres (Memoirs of the Bureau of Geological and Mining Research), no. 56, (Chapitre 4, Theorie de l'enchantillonnageequiprobable, pp. 42-51), Paris*.

Hadjigeorgiou, J & Lessard, J 2007, 'Numerical investigations of ore pass hang-up phenomena', *International Journal of Rock Mechanics and Mining Sciences*, vol. 44, issue 6, pp. 820–834, https://doi.org/10.1016/j.ijrmms.2006.12.006

Sneed, E & Folk, R 1958, 'Pebbles in the Lower Colorado River, Texas a study in particle morphogenesis', *Journal of Geology*, vol. 66, no. 2, pp. 114–150, http://www.jstor.org/stable/30058239

Vega, E, Espiñeira, D & Barindelli, G 2024, *Generación de Modelo Implícito de Unidades Geotécnicas Básicas Mina Chuquicamata 2024 (Generation of the Implicit Model of Basic Geotechnical Units Chuquicamata Mine 2024)*, Informe GRMD-SEG-INF-036/2024, Superintendencia de Estudios Geomecánicos, Gerencia de Recursos Mineros y Desarrollo, Mina Subterránea, División Chuquicamata de Codelco-Chile.

Vesilind, P 1980, 'The Rosin-Rammler Particle Size Distribution', *Resource Recovery and Conservation*, vol. 5, pp. 275–277.